

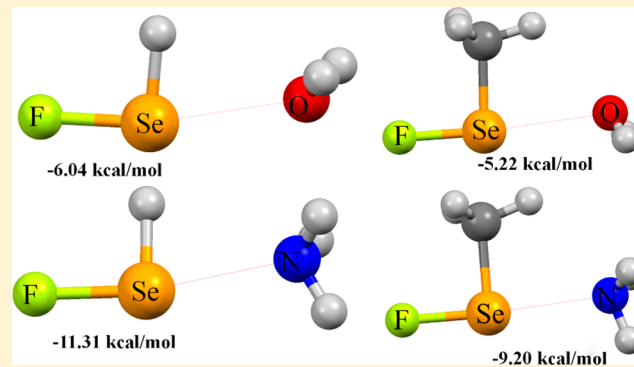
Exploring the Role of Substitution on the Formation of Se···O/N Noncovalent Bonds

Rahul Shukla and Deepak Chopra*

Crystallography and Crystal Chemistry Laboratory Department of Chemistry, Indian Institute of Science Education and Research Bhopal, Bhopal 462066, Madhya Pradesh, India

 Supporting Information

ABSTRACT: In this article, we have examined the effect of substitution on the formation of neutral $\text{XHSe}\cdots\text{O/N}$ ($\text{X} = -\text{H}, -\text{F}, -\text{CH}_3, -\text{CF}_3, -\text{Cl}, -\text{OH}, -\text{OCH}_3, -\text{NH}_2, -\text{NHC}_3, -\text{CN}$) noncovalent bonds with the oxygen atom from H_2O molecule and the nitrogen atom from NH_3 being the electron donor atoms, respectively. In addition to this, analysis has also been performed on $\text{XMeSe}\cdots\text{O/N}$ complexes to study the effect of the role of hydrogen bonding with the hydrogen atoms of the methyl group on $\text{Se}\cdots\text{O/N}$ interactions. Binding energy calculations were performed to determine the strength of these contacts. The obtained results establish the fact that the presence of a methyl group influences the strength of the observed $\text{Se}\cdots\text{O/N}$ interactions. Also in some cases, the $\text{O-H}\cdots\text{Se}$ interaction was observed to be more preferable over the $\text{Se}\cdots\text{O}$ interaction. The major contribution for stabilization of such $\text{Se}\cdots\text{O/N}$ interactions is from an interplay among the electrostatics and the exchange energy. To obtain deeper insights and understanding of such $\text{Se}\cdots\text{O/N}$ contacts, a topological analysis, using the QTAIM approach were also performed. This analysis showed that although the presence of a Me group modifies the $\text{Se}\cdots\text{O/N}$ interaction, it does not necessitate the formation of hydrogen bonds. To obtain insights into the orbital contributions, a natural bond orbital (NBO) analysis were performed which depicts that the strength of such interactions were derived via charge transfer from the oxygen/nitrogen lone pair to the σ^* orbital of the Se-X bond.



INTRODUCTION

The understanding of noncovalent interactions plays a very important role in the field of structural chemistry as well as biology.^{1–10} The most studied interaction in this regard are the hydrogen bonds which have garnered immense attention across different realms of chemistry and biology.^{11–17} Another important interaction, which is of significance to structural biology are the $\pi\cdots\pi$ stacking interactions and their presence in DNA, RNA, proteins and other macromolecules.^{18–22} In the past few years, in addition to the understanding of the nature of weak H-bonds, researchers have shifted their focus on the understanding of other related types of noncovalent interactions, such as halogen bonds,^{23–27} carbon bonds,^{28–30} chalcogen bonds,^{31–33} and pnicogen bonds.^{34–36} Studies have been performed to compare such interactions in order to obtain an improved understanding of their associated nature and energetics.^{37–40} Among them, the chalcogen bond defines a class of noncovalent interaction, in which a chalcogen atom is attracted noncovalently to a electronegative atom such as O or N but not only limited to these two.³¹ Interest in chalcogen bonds also stems from the presence of chalcogen atoms in biomolecules and plays an important role in determining the function of proteins,⁴¹ in the activation of thyroid hormones,⁴² having better antioxidant properties,⁴³ and in the detection of

biologically important analytes.⁴⁴ To enable an improved understanding of the role of the chalcogen atom, a complete understanding of the noncovalent interactions involving chalcogens is of importance. This is expected to provide insights into the design of molecules with specified properties containing these atoms as previous studies on the chalcogen atom have shown that it is capable of forming very strong intermolecular contacts and can function both as a bond acceptor and donor atom.^{45,46} Furthermore, it is also observed that sulfur is capable of forming both σ and hydrogen bond simultaneously in heterocyclic systems.⁴⁷

For an understanding of the role and importance of intermolecular interactions involving chalcogens, the atom selenium represents an ideal option because it plays an important role in chemistry as well as in biology. Selenium is a very important member of the chalcogen family because it has a soft metal-like behavior and also due to its applications in ligand chemistry^{48–51} and asymmetric synthesis.^{52–55} Also synthesis and biological applications of organoselenium have been well researched and documented.^{56–60} Selenium also

Received: September 5, 2015

Revised: October 10, 2015

Published: November 3, 2015

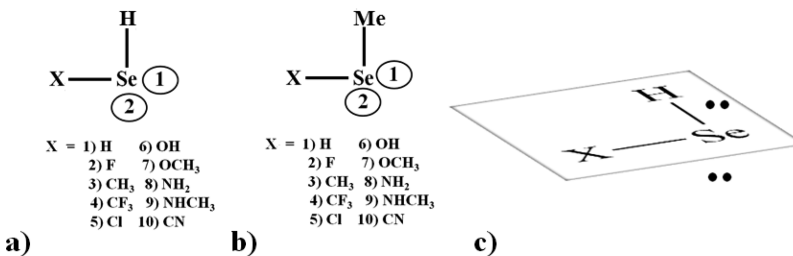


Figure 1. Schematic representation of (a) XHSe monomers, (b) XMeSe monomers, and (c) location of lone pairs on selenium.

plays a very important role in immune system,^{61–63} selenoproteins,^{64–66} and cancer therapy.^{67,68} On account of the immense potential and applications in the chemical and biological word, it was of interest to explore the formation of noncovalent bonds involving selenium.

The nature and role of the intramolecular Se···O and Se···N interaction has been studied extensively and is of potential relevance in organoselenium chemistry.^{69–73} The presence of an intermolecular interaction between Se and an electro-negative atom (O, N) has been established experimentally, with particular relevance to small molecules. Linden and co-workers have showed the presence of inter and intramolecular Se···O interactions in derivatives of diselenazole.⁷⁴ Espinosa and co-workers have further established the presence of an Se···O interaction by performing charge density analysis on selenium chalcogenophthalic anhydrides (SePA).⁷⁵ In another similar study, Guru Row and co-workers have showed the present of an unusually short Se···O interaction in the antioxidant molecule ebselen.⁷⁶ Studies performed on benzoselenadiazole establish that the presence of Se···N interactions are responsible for the observed optoelectronic properties. Crystal structure analysis on diaryl selenides have showed the presence of Se···N bonds⁷⁸ and an intermolecular dissymmetric [Se···N]₂ interaction was also observed in derivatives of chalcogenadiazoles.⁷⁹

The aim of this work was to systematically investigate the chalogen bond involving selenium. The role of substitution was analyzed to understand the nature of Se···O and Se···N bond by employing a model complex, XHSe···OH₂ and XHSe···NH₃. The substituents used for this study were X = -H, -F, -CH₃, -CF₃, -Cl, -OH, -OCH₃, -NH₂, -NHCH₃, and -CN. The occurrence of different substitutions will lead to a different electronic environment around the Se atom and is expected to alter the strength of the associated Se···O/N interaction. In addition to this, the strength of this interaction was also studied by the replacement of the H atom of XHSe with a methyl group. The electron donor atom will have an additional possibility of forming a hydrogen bond with the C-H bond of the methyl group and hence a systematic investigation of the energetics of this interaction has been performed.

COMPUTATIONAL METHODS

All the calculations have been performed at the second order Møller–Plesset theory (MP2)⁸⁰ using aug-cc-pVQZ level basis set.⁸¹ This level of theory provides reliable results and has been used in several studies of noncovalent interactions.^{38,39} Also results obtained from this basis set is found to be comparable with results obtained using computationally more expensive CCSD(T) level of theory using higher basis set.^{82–85} The structures were optimized using Gaussian 09 package.⁸⁶ All minima was verified to be a stationary point with no imaginary

frequencies. All further calculations were performed by utilizing the coordinates of the optimized structures. The molecular electrostatic potential (MEP) maps were plotted for the monomers participating in noncovalent interactions using G09. Binding energies were also computed to determine the strength of noncovalent interactions. The basis set superposition error was taken into account by the counterpoise correction.⁸⁷ The QTAIM provides a very good approach toward the topological understanding of noncovalent interactions by a systematic investigation of the electron density between two interacting atoms. The topological analysis was performed using AIMALL (version 13.05.06).⁸⁸ Selected topological parameters, such as the electron densities (ρ), Laplacian ($\nabla^2\rho$), local potential energy (V_b), and kinetic potential energy (G_b) at the bond critical point were obtained for all the noncovalent contacts. A second-order perturbation energy calculation was performed using Natural Bond Orbital (NBO) analysis^{89,90} at the DFT level with NBO6⁹¹ obtained by integrating with Gaussian 09. An energy decomposition analysis (EDA) was performed using GAMESS-US^{92,93} using the LMOEDA module in order to obtain the binding energies of the different complexes, and these were decomposed into the corresponding electrostatic, exchange, polarization, repulsion, and dispersion components, respectively. In the EDA methods, the difference between the energy of the supermolecule and the difference between the energy of the monomers constitute the total energy. The electrostatic energy is generally an attractive interaction which originates because of the interaction between the static charge densities of each monomers within the supermolecule. The stabilizing exchange energy arises from the asymmetric nature of the wave function which permits the exchange of electrons between monomers. The evaluation of the repulsion energy requires the energy to be expressed in terms of monomer orbitals that are orthonormal to each other. The polarization contribution is stabilizing and originates because of the relaxation of the supermolecular wave function. The dispersion energy is evaluated by computing the difference in the energy of the system calculated from MP2 approach and HF approach. The LMOEDA method has been applied extensively in the analysis of noncovalent interactions.^{94–96} The basis set for EDA analysis was obtained from the EMSL basis set library.^{97,98} To get a more deeper insight into the nature of the interaction, the electron density difference map were obtained for selected dimers using Multiwfn⁹⁹ and plotted using VMD.¹⁰⁰

RESULTS AND DISCUSSIONS

Molecular Electrostatic Potential (MEP) Maps. Molecular electrostatic potential maps were plotted for all the XHSe and XMeSe monomers on total density isosurface with electrostatic potential ranging from -12 kcal/mol (red) to 12

kcal/mol (blue) to analyze the effect of substitution on the electropositive and electronegative regions of selenium in XHSe monomers [Figure 1a] and XMeSe monomers [Figure 1b]. As shown in Figure 1, there are two possible electropositive regions on Se, one along the X–Se bond (marked as 1 and another along the H–Se bond (marked as 2), the lone pairs on selenium constitutes the electronegative region on selenium and is situated perpendicular to the plane defined by XHSe [Figure 1c]. Figure 2 shows the magnitude of region 1 of the

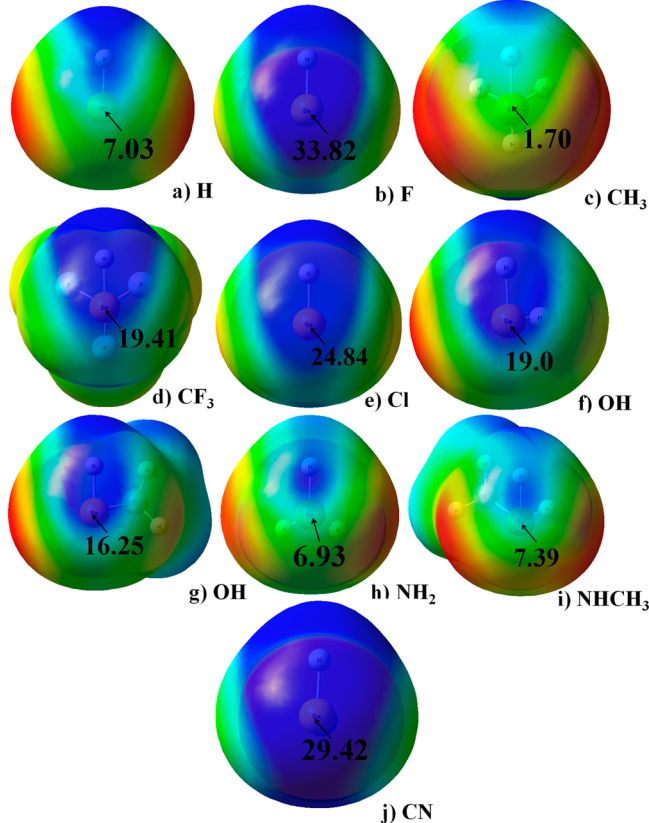


Figure 2. Electrostatic potential maps for region 1 of monomers (a) HSe , (b) FSe , (c) CH_3HSe , (d) CF_3HSe , (e) OHHSe , (f) OCH_3HSe , (g) NH_2HSe , (h) NHCH_3HSe , and (i) CNHSe on total density isosurface. Red and blue indicate electronegative and electropositive regions, respectively. All energy values are reported in kcal/mol.

XHSe monomers. The magnitude of the electropositive region on selenium was directly affected by the nature of the substituent X attached to selenium. For $\text{X} = -\text{H}$, the magnitude of 1 and 2 were same. The highest magnitude of 1 was obtained for $\text{X} = -\text{F}$ with a value of 33.82 kcal/mol followed by 29.42 kcal/mol for $\text{X} = -\text{CN}$ and 24.82 kcal/mol for $\text{X} = -\text{Cl}$. The high magnitude for these substituents was obtained because of the strong electron withdrawing nature of these substituents resulting in large electropositive region on selenium. For CF_3 , the magnitude of 1 was 19.41 kcal/mol closely followed by $\text{X} = -\text{OH}$. The magnitude of 1 for $\text{X} = -\text{OCH}_3$ decreased further to 16.93 kcal/mol. The electron withdrawing power of nitrogen is less compared to that of halogens and oxygen and this resulted in relatively lower value for $\text{X} = -\text{CH}_2$ and $-\text{NHCH}_3$ substituted monomers. As compared to 1, the magnitude of region 2 was less for all the substituents [Figure S1]. In case of $\text{X} = -\text{NHCH}_3$, the magnitude for region 2 was observed to be

negative (-3.40 kcal/mol). This negative value is because of the presence of lone pair of nitrogen in close vicinity. For XMeSe monomers, the magnitude of region 1 was lower as compared to those for the corresponding XHSe monomers for all the substituents [Figure 3]. This is because of the electron

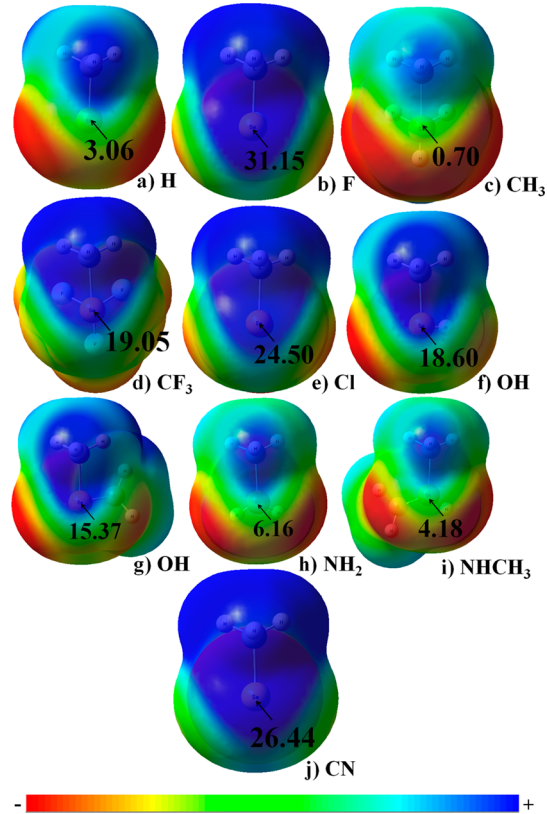


Figure 3. Electrostatic potential maps for region 1 of monomers (a) HMeSe , (b) FMeSe , (c) CH_3MeSe , (d) CF_3MeSe , (e) OHMeSe , (f) OCH_3MeSe , (g) NH_2MeSe , (h) NHCH_3MeSe , and (i) CNMeSe on total density isosurface. Red and blue indicates electronegative and electropositive regions, respectively.

donating behavior of the methyl group which results in the decrease in the magnitude of the electropositive region on selenium. Consequently, the magnitude of region 2 also decreased for all the substituents. In case of $\text{X} = -\text{NHCH}_3$, where region 2 becomes electropositive as compared to that of corresponding XHSe monomers because of the presence of the electron donating methyl group [Figure S2]. In terms of the magnitude of the electronegative region on the selenium atom, in most cases, the magnitude in case of XMeSe monomers [Figure S3] was larger than that of XHSe monomers [Figure S4]. The molecular electrostatic potential maps clearly shows that the noncovalent interaction involving selenium will be more favorable when the electron donating group is placed along the X–Se bond. Hence we have utilized this orientation for our study of $\text{Se}\cdots\text{O}/\text{N}$ noncovalent bond.

Understanding of XHSe···O Noncovalent Bonds. For this section, the molecular pairs were constructed by allowing the oxygen atom on the water molecule to interact with the selenium center. In all of the optimized structures, the $\text{Se}-\text{X}$ bond lies in the direction opposite to that of the oxygen atom. The presence of the hydrogen atom attached to the selenium atom in a perpendicular orientation avoids the possibility of any other competitive interaction and thus allowed for an

appropriate evaluation of the Se···O interaction. The water molecule was chosen because of its small size which enabled performing calculations at higher basis sets and hence directed toward obtaining results of improved accuracy. The optimized structures along with the related geometrical parameters and binding energies have been shown in Figure 4. All the

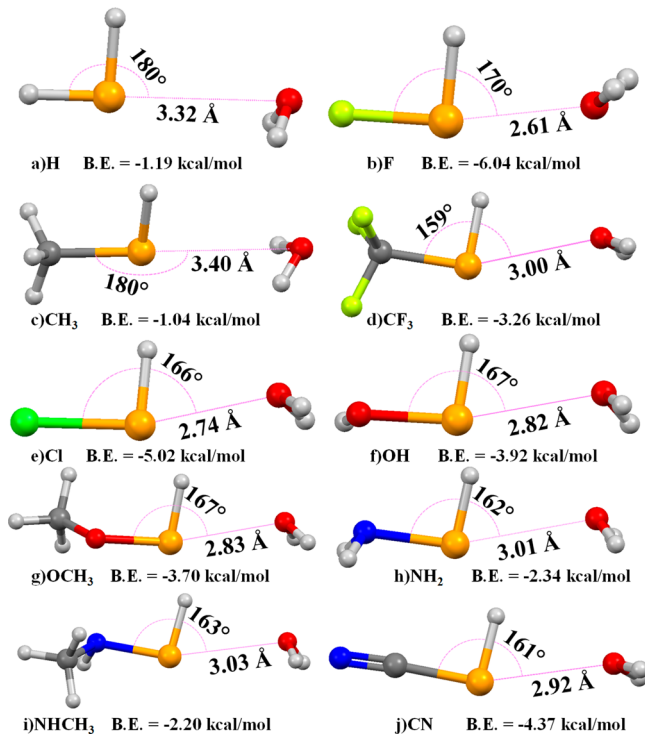


Figure 4. Optimized geometries of the $\text{XHSe}\cdots\text{OH}_2$ complex for $\text{X} =$ (a) $-\text{H}$, (b) $-\text{F}$, (c) $-\text{CH}_3$, (d) $-\text{CF}_3$, (e) $-\text{Cl}$, (f) $-\text{OH}$, (g) $-\text{OCH}_3$, (h) $-\text{NH}_2$, (i) $-\text{NHCH}_3$, (j) $-\text{CN}$.

structures shown in the figure corresponds to all the vibrational frequencies having real values, except in the case of $\text{X} = -\text{H}$ and $-\text{CH}_3$. In these two cases, the molecular pair with Se···O interaction and having all real frequencies was not observed and hence $\text{X}-\text{Se}\cdots\text{O}$ angle was fixed to 180° for the purpose of studying the Se···O interaction. A similar practice has been employed where a particular set of interaction with true minima was not observed for a given dimer.⁸⁵ Instead the true minima was observed with the dimer interacting via O-H···Se contact. These alternate structures with all real frequencies will be discussed in a separate section. The range for the Se···O distance ranges from 2.61 Å for $\text{X} = -\text{F}$ to 3.40 Å for $\text{X} = -\text{CH}_3$. The interaction was observed to be significantly

directional with the $\text{X}-\text{Se}\cdots\text{O}$ angle ranging from 159 to 170° (in case of $\text{X} = -\text{H}$ and $-\text{CH}_3$, the $\text{X}-\text{Se}\cdots\text{O}$ angle was fixed to 180°). In case of $\text{X} = -\text{H}$ and $-\text{CH}_3$, the oxygen atom was pointing away from the selenium atom because of which the calculated binding energy for these two dimers was calculated to be lowest with values of -1.19 and -1.04 kcal/mol, respectively. For all the other cases the oxygen atom points toward the selenium atom and hence leading to a more stabilized Se···O contact [Table 1]. On account of the Se···O distance being the shortest and the $\text{X}-\text{Se}\cdots\text{O}$ angle being highly directional in case of $\text{X} = -\text{F}$, it was expected, that the binding shall be strongest in this case. This assumption was confirmed by the value obtained from binding energy calculations [Table 1]. The energy values range between -1.04 kcal/mol for $\text{X} = -\text{CH}_3$ to -6.04 kcal/mol for $\text{X} = -\text{F}$. The substituents in terms of their binding energy are arranged in the following order: $-\text{CH}_3 \leftarrow \text{H} \leftarrow \text{NHCH}_3 \leftarrow \text{NH}_2 \leftarrow \text{CF}_3 \leftarrow \text{OCH}_3 \leftarrow \text{OH} \leftarrow \text{CN} \leftarrow \text{Cl} \leftarrow \text{F}$ [Figure 5]. The magnitude

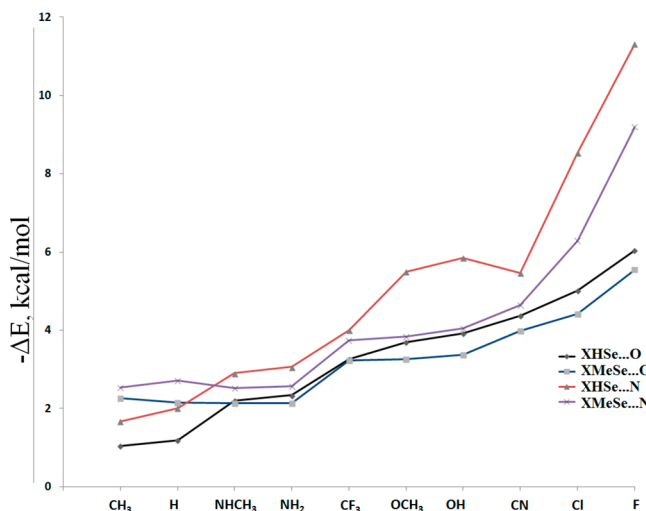


Figure 5. Binding energies of $\text{XHSe}\cdots\text{O}$, $\text{XMeSe}\cdots\text{O}$, $\text{XHSe}\cdots\text{N}$, and $\text{XMeSe}\cdots\text{N}$ complexes.

of the binding energy is also dependent on the electronegativity of the atom directly attached to Se. The strength increases in the order N < O < halogens. This is in accordance with the observation made from the molecular electrostatic potential maps. Greater the electron withdrawing power of the substituent X, greater will be the magnitude of the electro-positive region around selenium which will lead to a stronger Se···O noncovalent contact. For comparison, the binding energy for some representative dimer was also calculated at

Table 1. Geometrical Parameters, Binding Energies, Topological Parameters, and Charge Transfer Energies Obtained for Different $\text{XHSe}\cdots\text{O}$ Complexes

criteria	H	F	CH_3	CF_3	Cl	OH	OCH_3	NH_2	NHCH_3	CN
Se···O dist (Å)	3.32	2.61	3.40	3.00	2.74	2.82	2.83	3.01	3.03	2.92
X-Se···O angle (deg)	180	170	180	159	166	167	167	162	163	161
ΔE (kcal/mol)	-1.19	-6.04	-1.04	-3.26	-5.02	-3.92	-3.70	-2.34	-2.20	-4.37
BPL (Å)	3.330	2.612	3.419	2.997	2.742	2.825	2.839	3.014	3.033	2.923
ρ ($\text{e}/\text{\AA}^3$)	0.055	0.163	0.050	0.081	0.136	0.116	0.114	0.083	0.082	0.091
$\nabla^2\rho$ ($\text{e}/\text{\AA}^5$)	0.600	1.985	0.599	1.042	1.562	1.364	1.327	1.005	0.970	1.190
$\text{IV}_{\text{b}}/\text{G}_{\text{b}}$	0.873	0.988	0.809	0.881	0.980	0.964	0.964	0.914	0.919	0.886
$E(2)$ (kcal/mol)	1.06	11.48	0.65	3.06	8.85	6.90	6.96	3.75	3.73	3.98

Table 2. Counterpoise-Corrected Binding Energies of Some Representative Complexes at CCSD(T)/aug-cc-pvTZ and a Comparison with Those Computed at MP2/aug-cc-pvDZ Basis Set

	XHSe···OH ₂		XMeSe···OH ₂		XHSe···NH ₃		XMeSe···NH ₃	
	CCSD(T)	MP2	CCSD(T)	MP2	CCSD(T)	MP2	CCSD(T)	MP2
H	-1.41	-1.19	-2.49	-2.15	-2.11	-2.01	-2.91	-2.71
F	-5.89	-6.04	-5.39	-5.55	-10.63	-11.31	-9.29	-9.20

CCSD(T)/aug-cc-pvTZ basis set and it was observed that the energy were very much comparable to those obtained from MP2/aug-cc-pvDZ basis set [Table 2]. The energy decomposition analysis showed that the contribution for the stabilization of the Se···O interaction primarily comes from the exchange energy followed by the electrostatic energy (the percentage contribution toward the stabilization was calculated by adding the magnitude of electrostatics, exchange, polarizing, and dispersion energy components and then dividing the individual component with the total stabilization energy obtained) [Table S1]. This is in accordance with the results obtained for charge directed chalcogen bonds where electrostatic and exchange energies were among the dominating forces.¹⁰¹ In all the molecular pairs, the contribution of the exchange energy toward the stabilization of the Se···O interaction exceeded 45%, with the maximum being for X = -CH₃ (~49%). The percentage contribution of exchange energy was calculated to be maximum for X = -CN while was lowest for the X = -H. The percentage contribution for the polarization energy toward stabilization was higher for X = -F, -OH, -CF₃, and -NH₂ substituents as compared to the corresponding X = -H, -OCH₃, -CH₃, and -NHCH₃ substituents, respectively. Similarly the dispersion energy component was observed to be higher for X = -H and -CH₃ substituted dimers as compared to others. In general the contribution of the dispersion energy was lower for electron withdrawing groups.

The presence of such Se···O interactions was also confirmed by the presence of a bond critical point between selenium and oxygen [Figure S5]. The electron density values are in the range 0.050–0.163 e/Å³ [Table 1]. The lowest values of ρ were observed for X = -H and -CH₃ in which the X-Se···O angle was fixed to 180° while the highest values were obtained for the halogen atoms. The ρ value showed a exponential decay with increasing bond path length, a feature similar to those observed for weak hydrogen bonds [Figure 6]. The Laplacian ($\nabla^2\rho$) values obtained for this set of molecules were all positive,

ranging from 0.599 to 1.985 e/Å⁵ and showed similar trend to those observed for ρ values [Table 1] and it also showed an exponential decay with increasing bond path length [Figure 7].

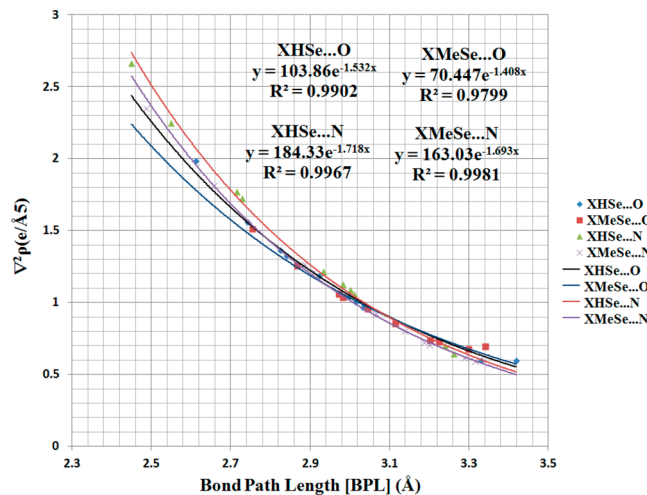


Figure 7. Plot showing variation of $\nabla^2\rho$ with increasing bond path length for different complexes of XHSe···O, XMeSe···O, XHSe···N, and XMeSe···N.

The trends in both ρ and $\nabla^2\rho$ followed a similar behavior as the binding energy as here also the respective values are dependent on the electronegativity of the atom attached to selenium. Similar to hydrogen bonds, the IV_bI/IG_bI ratios for all Se···O contacts were close to 1 for all the interacting dimers. As previously reported for other chalcogen bonds,³¹ Se···O values also follow related Koch and Popelier criteria set for hydrogen bonds and also were observed to be closed shell interactions.¹⁰²

As expected and previously reported for other chalcogen bonds,⁸⁵ the natural bond orbital analysis depicts that the charge transfer from the lone-pair of oxygen (O_{LP}) to the antibonding σ^* orbital of the Se–X bond is responsible for the strength of the Se···O interaction. The second-order perturbation energy E(2) was a maximum for X = -F with a value of 11.48 kcal/mol while it was a minimum for X = -CH₃ [Table 1]. E(2) does not follow the same trend as observed in case of the binding energy. The reason for this behavior can be explained by the different approach by which these two values are calculated. While the binding energy is calculated between considering the basis set of the entire monomers involved in the interaction, the E(2) values just refers to a specific pairs of orbitals. The magnitude of E(2) increased in the order -CH₃ < -H < -CF₃ < -NHCH₃ < -NH₂ < -CN < OH < -OCH₃ < -Cl < -F. Even though the trends in magnitudes of E(2) are not similar to the total binding energy, a comparison with the different energy components obtained from the decomposition analysis largely follows the trends observed for the magnitudes of the electrostatic and the exchange energy components. One of the exception was the E(2) value for X = -CF₃, which was lower than the corresponding values observed

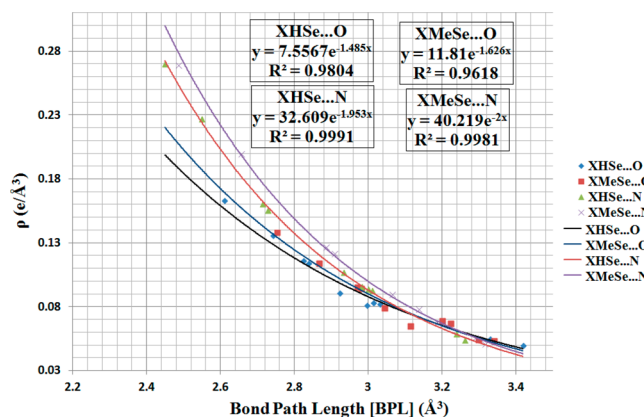


Figure 6. Plot showing variation of ρ with increasing bond path lengths for different complexes of XHSe···O, XMeSe···O, XHSe···N, and XMeSe···N.

for $X = -\text{NH}_2$ and $-\text{NHCH}_3$ substituents. It is also worthy to note that the trend observed for the repulsion energy component was similar to the trend observed for $E(2)$. Since exchange energy and electrostatic energy were the dominating forces, it can be concluded that these two forces are responsible for the charge transfer from the lone-pair of oxygen (O_{LP}) to the antibonding σ^* orbital of the $\text{Se}-\text{X}$ bond.

Understanding of XMeSe···O Noncovalent Bonds. For this set of molecules, the hydrogen atom of the HXSe molecule was replaced with a Me group. The purpose was to study the energetics associated with $\text{Se} \cdots \text{O}$ interaction, in the event of the oxygen atom having an alternative option of forming a hydrogen bond with the C–H bond of the methyl group. The optimized structures along with the relevant geometrical parameters and binding energies have been shown in Figure 8.

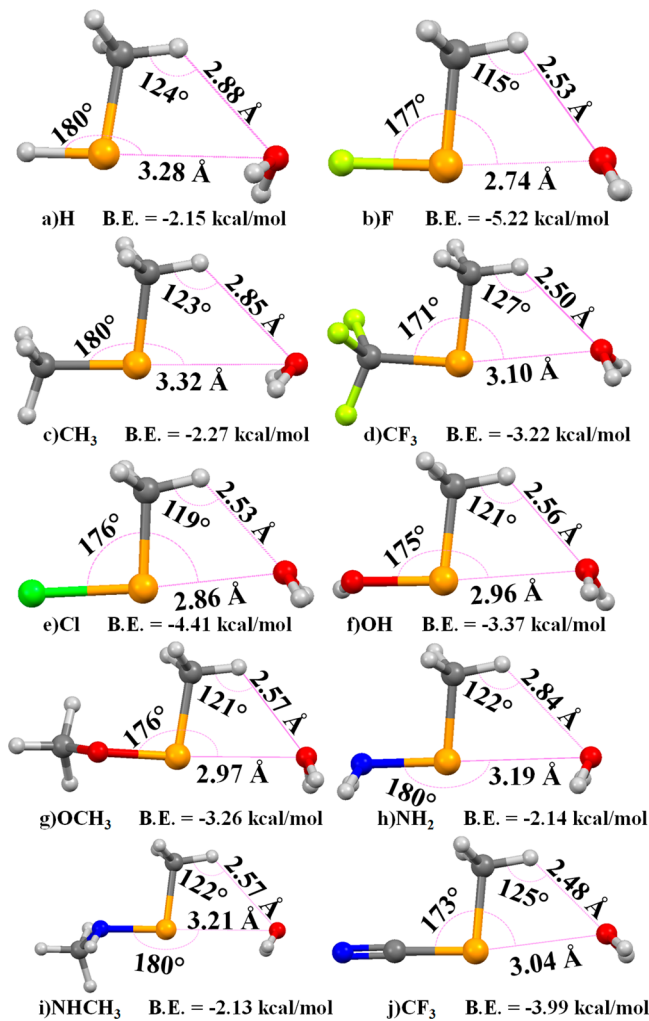


Figure 8. Optimized geometries of the $\text{XMeSe} \cdots \text{OH}_2$ complex for $X =$ (a) $-\text{H}$, (b) $-\text{F}$, (c) $-\text{CH}_3$, (d) $-\text{CF}_3$, (e) $-\text{Cl}$, (f) $-\text{OH}$, (g) $-\text{OCH}_3$, (h) $-\text{NH}_2$, (i) $-\text{NHCH}_3$, and (j) $-\text{CN}$.

In this section, apart from $X = -\text{H}$ and $-\text{CH}_3$, true minima for the molecular pair with $X = -\text{NH}_2$ and $-\text{NHCH}_3$ forming the $\text{Se} \cdots \text{O}$ interaction was not observed. This observation is in accordance with the low magnitude of the electropositive region observed for monomers with $X = -\text{NH}_2$ and $-\text{NHCH}_3$ [Figure 2] and further decrease in its magnitude with the introduction of a methyl group [Figure 3]. These structures with true minima will be discussed in another

section. For the purpose of studying $\text{Se} \cdots \text{O}$ contacts, here also the $\text{X}-\text{Se} \cdots \text{O}$ angle was fixed to 180° . There was an increase in the $\text{Se} \cdots \text{O}$ distance for the molecular pairs in comparison to that of $\text{XHSe} \cdots \text{O}$ pairs (except for $X = -\text{H}$ and $-\text{CH}_3$). Interestingly, there was an associated increase in angularity, with the $\text{X}-\text{Se} \cdots \text{O}$ angle greater than 170° for each of the molecular pairs [Table 3]. Here also the oxygen atom of H_2O points away from the selenium atom for the dimers in which $\text{X}-\text{Se} \cdots \text{O}$ angle was fixed to 180° . The binding energies ranged from -2.13 kcal/mol ($X = -\text{NHCH}_3$) to -5.22 kcal/mol ($X = -\text{F}$) but the trends were not similar in comparison to those observed for a $\text{XHSe} \cdots \text{O}$ interaction [Table 3]. There was decrease in the binding energy for all the molecular pairs, except for $X = -\text{H}$ and $X = -\text{CH}_3$, wherein the binding energy increased substantially in comparison to the $\text{XHSe} \cdots \text{O}$ pairs [Figure 5]. Hence it can be concluded that hydrogen bonding was more stabilizing than the $\text{Se} \cdots \text{O}$ contact in the case of $X = -\text{H}$, $-\text{CH}_3$. For $X = -\text{H}$, $-\text{CH}_3$, $-\text{NH}_2$, and $-\text{NHCH}_3$, the $\text{Se} \cdots \text{O}$ distance was nearly the same for $\text{XMeSe} \cdots \text{O}$ contacts in which $\text{X}-\text{Se} \cdots \text{O}$ angle was fixed to 180° . Also for $X = -\text{CF}_3$, the binding energy for $\text{XHSe} \cdots \text{O}$ and $\text{XMeSe} \cdots \text{O}$ dimer was nearly equal [Figure 5]. The above-mentioned changes in binding energy and geometrical features of $\text{Se} \cdots \text{O}$ contacts were on account of the possibility of the presence of $\text{C}-\text{H} \cdots \text{O}$ interactions. The $\text{H} \cdots \text{O}$ distances ranged between 2.48 and 2.93 \AA and $\text{C}-\text{H} \cdots \text{O}$ angle is in the range of 119 – 127° [Figure 5, Table S5]. These geometrical parameters were in line with the definition suggested by IUPAC for hydrogen bonding.¹⁰³ As reported for the previous section, the energy decomposition analysis (EDA) showed that the exchange energy dominated, with at least 46% contribution toward the stabilization of the $\text{Se} \cdots \text{O}$ interaction followed by an electrostatic contribution, with at least 26% contribution toward the total stabilization [Table S2]. With the introduction of an additional methyl group, the percentage contribution from the exchange energy toward the stabilization increased, as compared to $\text{XHSe} \cdots \text{O}$ interactions. The electrostatic energy contribution decreased for all the pairs except for $X = -\text{H}$. The contribution from polarization energy decreased only in the case of $X = -\text{H}$ while the increased contribution from dispersion energy was observed only in case of $X = -\text{CH}_3$ [Table S2].

A topological analysis performed on the complexes in this section gave some interesting results with regard to the introduction of the $-\text{Me}$ group. Although the geometrical parameters indicated the presence of hydrogen bonding between the oxygen and the hydrogen atom of the Me group, a topological analysis suggested that this is not always the case. This is because no bcp was observed between oxygen and hydrogen when $X = -\text{F}$, $-\text{NH}_2$, $-\text{NHCH}_3$ [Figure S6]. While absence of a bcp between O and H for $X = -\text{F}$ can be attributed to the presence of the electronegativity of fluorine which lead to formation of a strong $\text{Se} \cdots \text{O}$ interaction. In case of $X = -\text{NH}_2$ and $-\text{NHCH}_3$, the absence of a bcp between H and O can be because selenium and oxygen in those pairs were forced to interact as a consequence of which no bcp was observed between oxygen and hydrogen. The value of ρ ranges from $0.053 \text{ e}/\text{\AA}^3$ ($X = -\text{CH}_3$) to $0.138 \text{ e}/\text{\AA}^3$ ($X = -\text{F}$) for $\text{Se} \cdots \text{O}$ interaction [Table 3] while the values of ρ ranges from $0.029 \text{ e}/\text{\AA}^3$ ($X = -\text{CH}_3$) to $0.065 \text{ e}/\text{\AA}^3$ ($X = -\text{CN}$) for the $\text{O} \cdots \text{H}$ interactions [Table S5]. For $X = -\text{H}$ and $-\text{CH}_3$, the values of ρ observed for $\text{O} \cdots \text{H}$ were significantly less than those observed for other substituents. The $\nabla^2\rho$ value ranges from $0.679 \text{ e}/\text{\AA}^5$ ($X = -\text{H}$) to $1.515 \text{ e}/\text{\AA}^5$ ($X = -\text{F}$) for $\text{Se} \cdots \text{O}$ interactions

Table 3. Geometrical Parameters, Binding Energies, Topological Parameters, and Charge Transfer Energies Obtained for Different XMeSe \cdots O Complexes

criteria	H	F	CH ₃	CF ₃	Cl	OH	OCH ₃	NH ₂	NHCH ₃	CN
Se \cdots O dist (Å)	3.28	2.74	3.32	3.10	2.86	2.96	2.97	3.19	3.21	3.04
X \cdots Se \cdots O angle (deg)	180	177	180	171	176	175	176	180	180	173
ΔE (kcal/mol)	-2.15	-5.55	-2.27	-3.22	-4.41	-3.37	-3.26	-2.14	-2.13	-3.99
BPL (Å)	3.298	2.754	3.341	3.114	2.867	2.971	2.982	3.201	3.224	3.044
ρ (e/Å ³)	0.054	0.138	0.053	0.065	0.114	0.095	0.094	0.069	0.067	0.079
$\nabla^2\rho$ (e/Å ⁵)	0.679	1.515	0.697	0.857	1.260	1.066	1.042	0.743	0.730	0.963
IV _b J/G _b	0.839	1.007	0.807	0.862	0.974	0.958	0.961	0.926	0.914	0.897
E(2) [kcal/mol]	1.00	9.06	0.85	2.37	6.47	4.60	4.62	1.99	1.76	3.01

[Table 3] while the values for the $\nabla^2\rho$ ranges from 0.446 ($X = -\text{CH}_3$) to 0.851 ($X = -\text{CN}$) for the O \cdots H interaction [Table S5]. The values of ρ and $\nabla^2\rho$ for Se \cdots O contacts was higher than the corresponding values for O \cdots H contact in the same dimer. Comparing the ρ and $\nabla^2\rho$ for XMeSe \cdots O with that observed for XHSe \cdots O [Figure 6, Figure 7], it was clearly evident that due to the presence of a C–H bond in the close vicinity, a minor portion of the electron density on oxygen was directed toward hydrogen which resulted in the lowering of the ρ and $\nabla^2\rho$ values for the Se \cdots O bond. This lowering of the topological parameters was even observed for $X = -\text{F}$, $-\text{NH}_2$, and $-\text{NHCH}_3$ even though no bcp was observed between oxygen and hydrogen in XMeSe \cdots O complex.

NBO analysis showed that the E(2) value for transition from O_{LP} to antibonding σ^* orbital of Se–X ranges from 0.85 to 9.06 kcal/mol [Table 3]. These energies values were considerably lower than those observed for the corresponding XHSe \cdots O interactions [Table 1]. The reason for the lowering of E(2) values could be ascribed to the possibility of formation of the H \cdots O interaction. NBO analysis also confirmed this feature on account of the observed transition between the oxygen lone pair and the antibonding orbital of the C–H bond [Table S5]. In each complex, the E(2) contribution from O_{LP} to the antibonding σ^* orbital of the C–H bond was lower than the corresponding values observed for O_{LP} to the antibonding σ^* orbital of the Se–X bond. Comparing the trends in the magnitude of E(2) with those of the different energy components reveals that both the electrostatic and polarization energy component follows the same trend as of E(2) and the exchange energy also followed the same trend with the exception of $X = -\text{CF}_3$.

Understanding of XHSe \cdots N Noncovalent Bonds. For this section, the molecular pairs were constructed by allowing the nitrogen atom on the ammonia molecule to interact with selenium. Similar to water, ammonia is also a small molecule with one lone pair and has been extensively used in previous studies.⁸² The optimized structures along with the geometrical parameters and binding energies are shown in Figure 9. In case of XHSe \cdots N interactions, we obtained all the dimers forming Se \cdots N interaction and having true minima. The Se \cdots N distance ranges from 2.45 to 3.24 Å and all X–Se \cdots N angles were in the range of 164–172°. The binding energy increased in the order $-\text{CH}_3 \leftarrow \text{H} \leftarrow \text{NHCH}_3 \leftarrow \text{NH}_2 \leftarrow \text{CF}_3 \leftarrow \text{CN} \leftarrow \text{OCH}_3 \leftarrow \text{OH} \leftarrow \text{Cl} \leftarrow \text{F}$. In this case, due to the presence of short Se \cdots N distance and high angularity of X–Se \cdots N angle, $X = -\text{F}$ has the highest binding energy of -11.31 kcal/mol while $X = -\text{CH}_3$ has the lowest binding energy of -1.67 kcal/mol [Table 4]. The energy decomposition analysis revealed that the stability of the Se \cdots N interaction was mainly because of the exchange energy, with the percentage contribution greater than 45%

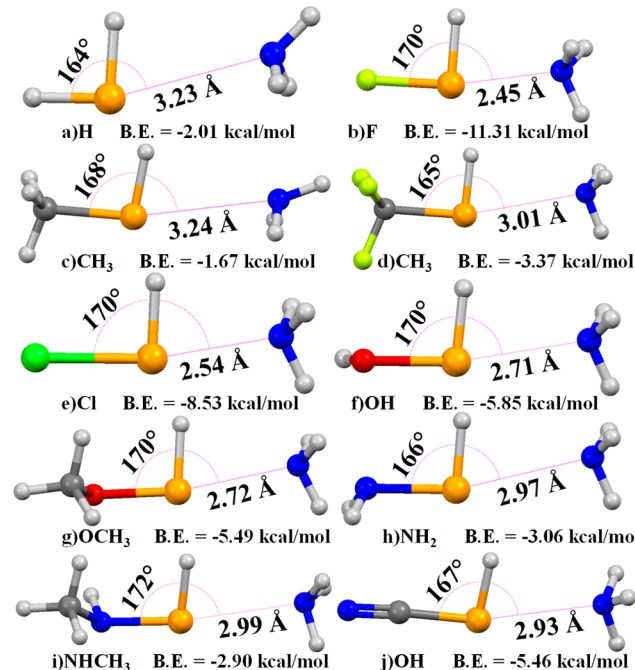


Figure 9. Optimized geometries of the XHSe \cdots NH₃ complex for X = (a) $-\text{H}$, (b) $-\text{F}$, (c) $-\text{CH}_3$, (d) $-\text{CF}_3$, (e) $-\text{Cl}$, (f) $-\text{OH}$, (g) $-\text{OCH}_3$, (h) $-\text{NH}_2$, (i) $-\text{NHCH}_3$, and (j) $-\text{CN}$.

followed by the electrostatic energy with at least 32% contribution toward stability [Table S3]. The polarization and the dispersion energy contribution was relatively small as compared to the exchange or electrostatic energy but their contribution directly depends on the electron donating or electron withdrawing effects of the substituent X. Strong electron withdrawing groups resulted in lower dispersion energy contribution and concomitant high contribution to the polarization energies [Table S3].

A topological analysis showed that the presence of a bcp between selenium and nitrogen for each of the complexes [Figure S7]. The ρ values ranged from 0.054 to 0.270 e/Å³ and increased in the order $-\text{CH}_3 \leftarrow \text{H} \leftarrow \text{CF}_3 \leftarrow \text{NHCH}_3 \leftarrow \text{NH}_2 \leftarrow \text{CN} \leftarrow \text{OCH}_3 \leftarrow \text{OH} \leftarrow \text{Cl} \leftarrow \text{F}$. The $\nabla^2\rho$ values ranges from 0.644 e/Å⁵ to 2.663 e/Å⁵. Both ρ and $\nabla^2\rho$ followed the law of exponential decay with increasing bond path length [Figure 6, Figure 7]. Similar to Se \cdots O, Se \cdots N interaction also follows the Koch and Popelier criteria and was observed to be a closed shell interaction, a feature similar to other chalcogen bonds.

For the Se \cdots N interaction, the charge transfer process takes place from N_{LP} to the antibonding σ^* Se–X bond. The second-order perturbation energy was highest for $X = -\text{F}$

Table 4. Geometrical Parameters, Binding Energies, Topological Parameters, and Charge Transfer Energies Obtained for Different XHSe \cdots N Complexes

criteria	H	F	CH ₃	CF ₃	Cl	OH	OCH ₃	NH ₂	NHCH ₃	CN
Se \cdots N dist (Å)	3.23	2.45	3.24	3.01	2.54	2.71	2.72	2.97	2.99	2.93
X–Se \cdots N angle (deg)	164	170	168	165	170	170	170	166	172	167
ΔE (kcal/mol)	-2.01	-11.31	-1.67	-4.00	-8.53	-5.85	-5.49	-3.06	-2.90	-5.46
BPL (Å)	3.239	2.450	3.262	3.011	2.549	2.714	2.728	2.982	3.000	2.933
ρ (e/Å ³)	0.059	0.270	0.054	0.093	0.227	0.161	0.156	0.096	0.094	0.107
$\nabla^2\rho$ (e/Å ⁵)	0.700	2.663	0.644	1.056	2.251	1.771	1.726	1.128	1.088	1.214
IV ₂ J/G _b	0.840	1.103	0.843	0.885	1.051	0.971	0.965	0.888	0.886	0.900
E(2) [kcal/mol]	1.78	32.06	1.22	5.43	25.47	14.92	14.72	6.33	5.96	7.06

(32.06 kcal/mol) and the lowest for X = -CH₃ (1.22 kcal/mol) [Table 4]. The E(2) energy values for different substitutions followed the same trend as observed for ρ . Furthermore, E(2) followed the same trend as that of electrostatics and the exchange energy components. One exception was X = -CF₃ whose magnitude of E(2) was lower than X = -NH₂ and -NHCH₃ substituent but the binding energy was higher for X = -CF₃. This trends suggests that similar to Se \cdots O contacts, the charge transfer from N_{LP} to the antibonding σ^* Se–X bond is governed by electrostatic character.

Understanding of XMeSe \cdots N Noncovalent Bonds. In order to study the effect of methylation on the nature of the Se \cdots N with varying X group, the hydrogen of the XHSe group was replaced with a Me group. True minima was observed for all the dimers involved in Se \cdots N contact. The optimized geometries along with the relevant geometrical parameters are shown in Figure 10. The Se \cdots N distance ranges from 2.48 Å for X = -F to 3.27 Å for X = -H. The Se \cdots N distance for XMeSe \cdots NH₃ were higher than those observed for XHSe \cdots NH₃ complexes. The X–Se \cdots N angularity ranged from 174 to 178° [Table 5]. Beside Se \cdots N interactions, there exists the possibility of formation of the C–H \cdots N interaction [since H \cdots N distance ranges from 2.64 to 2.77 Å which was closer to the sum of the vdW radii of hydrogen and nitrogen [Table S6]. Also C–H \cdots N angles were greater than 110° (except for X = -F where no C–H \cdots N contact was observed) and hence satisfy the criteria for hydrogen bonding [Table S6]. The binding energies ranged from -2.52 kcal/mol for X = -NHCH₃ to -9.20 kcal/mol for X = -F. Except for X = -H and -CH₃, there was a decrease in the binding energy of XMeSe \cdots N pairs as compared to the values observed for XHSe \cdots N pairs [Table 5]. Energy decomposition analysis showed that in comparison to XHSe \cdots N interaction, their was an increase in the exchange energy component for all the pairs of XMeSe \cdots N and similarly their was decrease in the percentage contribution of electrostatic component toward stabilization [Table S4]. In terms of the polarizability energy, their was a increase in the percentage contribution for all the pairs and their was a increase in the dispersion energy component for all the pairs except for X = -F, -Cl, -OH, -OCH₃ which happens to be the strong electron withdrawing groups[Table S4].

The presence of these interactions were confirmed by the presence of a bond critical point between selenium and nitrogen [Figure S8]. Topological analysis showed that there was an increase in the bond path length between selenium and nitrogen when the hydrogen of XHSe was replaced by Me. Beside the observation of a bcp between selenium and nitrogen, a bcp was also observed between oxygen and nitrogen for all the pairs except for X = -F, -Cl, -OH, and -OCH₃. In the case of X = -F, the C–H bond was not directed toward the

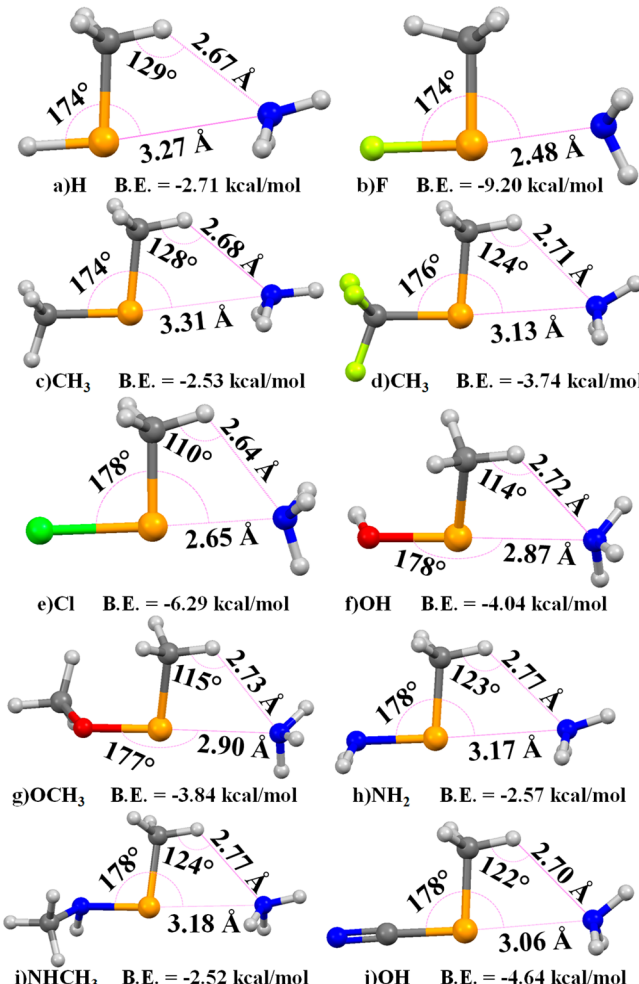


Figure 10. Optimized geometries of the XMeSe \cdots NH₃ complex for X = (a) -H, (b) -F, (c) -CH₃, (d) -CF₃, (e) -Cl, (f) -OH, (g) -OCH₃, (h) -NH₂, (i) -NHCH₃, and (j) -CN.

nitrogen and hence no bond between oxygen and hydrogen was possible, and hence it was expected that no BCP will be observed. However, in case of X = -Cl, -OH, and -OCH₃, no bcp was observed even though the criteria for hydrogen bonding were satisfied. This indicates that mere fulfillment of the geometrical criteria for hydrogen bonding does not necessarily lead to a interaction and hence the spatial orientation of the interacting atom within the molecule is also important. The presence of a Me group directly affects the value of ρ and $\nabla^2\rho$. The topological values observed for these two parameters in case of the XMeSe \cdots N interactions were

Table 5. Geometrical Parameters, Binding Energies, Topological Parameters, and Charge Transfer Energies Obtained for Different XMeSe \cdots N Complexes

criteria	H	F	CH ₃	CF ₃	Cl	OH	OCH ₃	NH ₂	NHCH ₃	CN
Se \cdots N dist (Å)	3.27	2.48	3.31	3.13	2.65	2.87	2.90	3.17	3.18	3.06
X–Se \cdots N angle (deg)	174	174	174	176	178	178	177	178	178	178
ΔE (kcal/mol)	-2.71	-9.20	-2.53	-3.74	-6.29	-4.04	-3.84	-2.57	-2.52	-4.64
BPL (Å)	3.289	2.487	3.316	3.138	2.657	2.886	2.909	3.187	3.200	3.065
ρ (e/Å ³)	0.056	0.269	0.051	0.078	0.200	0.127	0.122	0.068	0.066	0.090
$\nabla^2\rho$ (e/Å ⁵)	0.619	2.350	0.593	0.806	1.815	1.268	1.216	0.725	0.707	0.927
IV _b J/G _b	0.867	1.123	0.857	0.904	1.035	0.954	0.948	0.894	0.892	0.909
E(2) [kcal/mol]	1.70	27.72	1.51	2.42	15.28	8.33	7.88	1.63	1.48	3.69

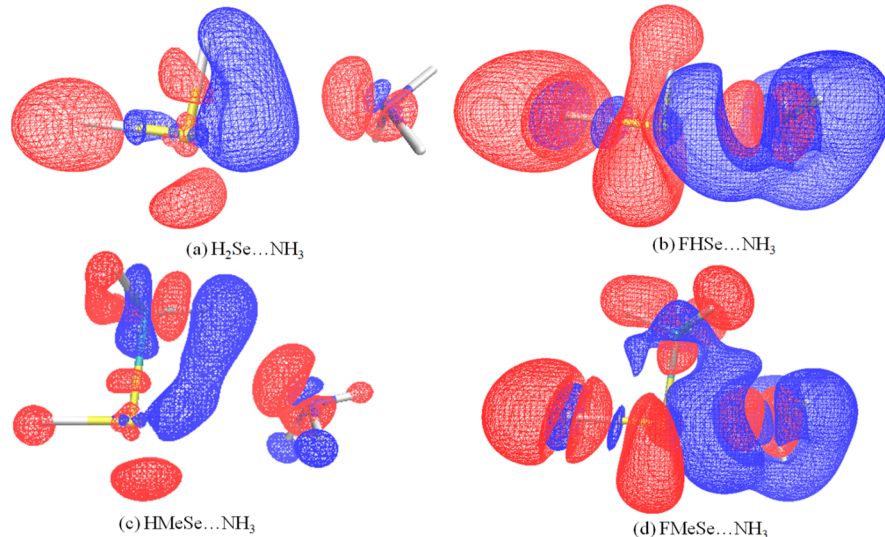


Figure 11. Electron density shift occurring in (a) H₂Se \cdots NH₃, (b) FHSe \cdots NH₃, (c) HMeSe \cdots NH₃, and (d) FMeSe \cdots NH₃. Red and blue region depicts the gain and loss of density, respectively. All shifts are mapped with 0.0005 au contours.

significantly lower than the corresponding value observed for XHSe \cdots N interaction [Table 5]

There is a significant decrease in the observed values of $E(2)$ for the LP_N transition to the Se–X σ^* orbital due to the presence of a Me group [Table 5]. Again the NBO results were exactly complementary to the results obtained from the topological analysis. Besides the occurrence of a LP_N to Se–X σ^* orbital transition, significant values for the LP_N to C–H σ^* orbital transitions were also observed. The lowest value for LP_N to C–H σ^* orbital transitions were observed for X = –F (0.59 kcal/mol), –Cl (0.43 kcal/mol), –OCH₃ (0.63 kcal/mol), –OH (0.59 kcal/mol) [Table S6] and it is indeed noteworthy that these were the same pairs where no bcp was observed between the nitrogen and the selenium atom. The remaining part of the molecular pair showed $E(2)$ of more than 1 kcal/mol for transition from LP_N to C–H σ^* orbital suggesting substantial charge transfer in case of hydrogen bonding. As observed in the previous sections, here also the charge transfer from the LP_N transition to the Se–X σ^* bond mainly follows the trends of electrostatic and exchange energy components.

In the study involving such complexes, the electron density shift can provide meaningful insights about the characteristics of these interactions. The shifts indicates the difference between the density of the complex to the sum of isolated monomers. Figure 11 shows the density of Se \cdots N complexes. Red areas represents the increased density and blue area represent the decreased density in the complex.

In all the four complexes represented in Figure 11, an increase in the electron density is observed on the N lone pair and a decrease in the electron density is observed for the Se atom which functions as a electron acceptor. Also there is an increase in the charge on the far side of the Se–X bond in all the cases. This buildup of charge is more in the case of Figure 11, parts a and b, as compared to Figure 11, parts c and d. Incase of fluorine substituted dimers, the charge depleted region of Se and N coalesce into one and surround the charge enhanced region of NH₃ molecule resulting in strongest Se \cdots O contact.

Alternative Minima in the Formation of the Complex. In case of Se \cdots O interactions, as mentioned previously true minima was not obtained for few dimers. In case of systems involving XHSe, X = –H and –CH₃, favored the formation of hydrogen bonding, i.e., O–H \cdots Se interaction with the water molecule rather than Se \cdots O interaction. The structure of these true minima has been shown in Figure 12. The H \cdots Se distance was observed to be 2.65 Å for X = –H and –CH₃ respectively. The O–H \cdots Se angle was 167° and 149° respectively. For X = –CH₃, apart from O–H \cdots Se interaction, the oxygen atom was also involved in the formation of a weak C–H \cdots O interaction 2.62 Å/120°. The binding energy for H₂Se/H₂O and CH₃HSe/H₂O involved in hydrogen bonding was also greater than the corresponding dimer involved in Se \cdots O contact [Table 1, Figure 12]. The topological analysis [Figure S9] also provides pointers toward the higher stability of these alternative true minima. The ρ and $\nabla^2\rho$ values obtained for the H \cdots Se contact

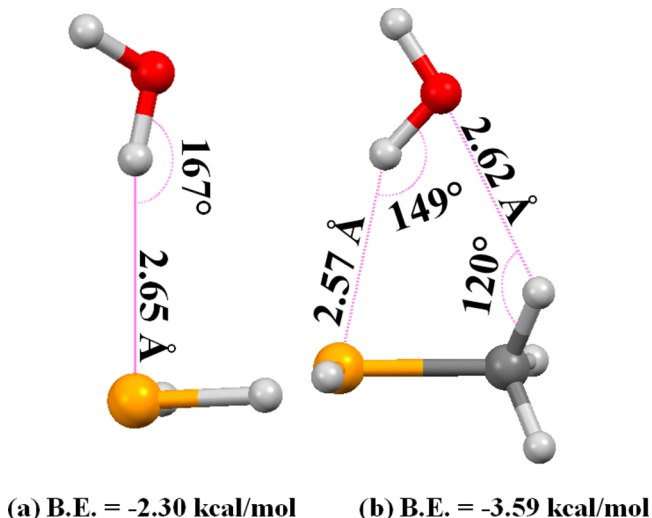


Figure 12. Optimized structure of (a) $\text{H}_2\text{Se}\cdots\text{H}_2\text{O}$ and (b) $\text{CH}_3\text{HSe}\cdots\text{H}_2\text{O}$ having true minima.

in these dimers were higher than those observed for the corresponding $\text{Se}\cdots\text{O}$ contact [Table 6].

Table 6. Topological Parameters for the Optimized Structure of $\text{H}_2\text{Se}/\text{H}_2\text{O}$ and $\text{CH}_3\text{HSe}/\text{H}_2\text{O}$ Having True Minima

interaction	ρ ($\text{e}/\text{\AA}^3$)	$\nabla^2\rho$ ($\text{e}/\text{\AA}^3$)
$\text{H}\cdots\text{Se}$	$\text{H}_2\text{Se}\cdots\text{H}_2\text{O}$	0.694
	0.087	
$\text{H}\cdots\text{Se}$	0.104	0.853
$\text{O}\cdots\text{H}$	0.045	0.719

The electron density difference map [Figure 13] plotted depicts that in case of $\text{O}-\text{H}\cdots\text{Se}$ interaction, there is an increase

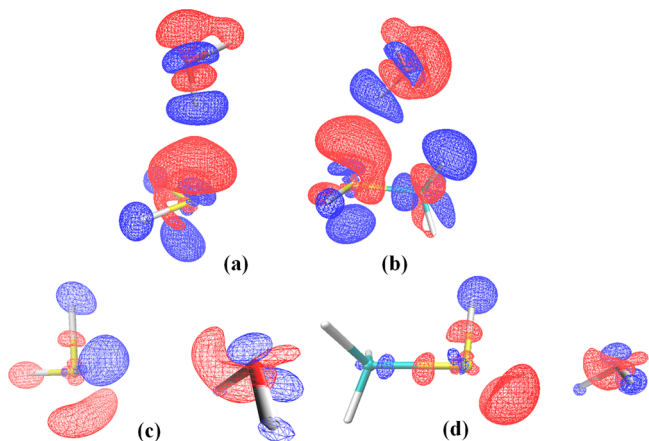


Figure 13. Electron density shift for hydrogen bonding in (a) $\text{H}_2\text{Se}/\text{OH}_2$ and (b) $\text{CH}_3\text{HSe}/\text{OH}_2$ and $\text{Se}\cdots\text{O}$ contact in (c) $\text{H}_2\text{Se}/\text{OH}_2$ and (d) $\text{CH}_3\text{HSe}/\text{OH}_2$.

in the density observed on the sulfur lone pair when the complex is formed due to hydrogen bonding. This increase is accompanied by a substantial decrease in the charge on the hydrogen on H_2O . In case of $\text{CH}_3\text{HSe}\cdots\text{H}_2\text{O}$ complex [Figure 13b], additionally there is a substantial increase in charge

around the oxygen lone pair accompanied by a decrease in the charge around the C–H bond resulting in the formation of a weak $\text{C}-\text{H}\cdots\text{O}$ interaction. In case of Figure 13c, a small increase in density around the oxygen lone pair is accompanied by a decrease in density around selenium resulting in $\text{Se}\cdots\text{O}$ contact but in Figure 13d, a decrease in density around selenium is not visible at this contour level, resulting in a weaker $\text{Se}\cdots\text{O}$ contact. The large size of the contours in Figure 13, parts a and b, as compared to in Figure 13, parts c and d, clearly shows that the $\text{O}-\text{H}\cdots\text{Se}$ contact was more preferable than $\text{Se}\cdots\text{O}$ contact in these cases.

In case of molecules involving XMeSe , apart from $\text{X} = -\text{H}$ and $\text{X} = -\text{CH}_3$, dimers with $\text{X} = -\text{NH}_2$ and $-\text{NHCH}_3$ also preferred the formation of a $\text{O}-\text{H}\cdots\text{Se}$ interaction. The reason for this behavior can be attributed to the following observations.

- 1 Replacement of a H with Me, further decreases the electropositive region around Se and/or increases the electronegative region around Se for $\text{X} = -\text{NH}_2$ and $-\text{NHCH}_3$, which results in the hydrogen atoms of the water molecule having the required orientation to participate in hydrogen bond formation rather than the formation of the $\text{Se}\cdots\text{O}$ interaction.
- 2 Apart from $\text{O}-\text{H}\cdots\text{Se}$, the oxygen atom of the water molecule is also involved in the formation of strong $\text{N}-\text{H}\cdots\text{O}$ hydrogen bond.
- 3 The binding energy of $\text{N}-\text{H}\cdots\text{O}/\text{O}-\text{H}\cdots\text{Se}$ interaction is greater than $\text{Se}\cdots\text{O}$ interaction [Figure 14] and also the topological parameters observed for hydrogen bonded dimers were higher than those obtained for the corresponding $\text{Se}\cdots\text{O}$ contacts [Figure S10, Table 7].

Herein also, the electron density difference plot [Figure 15] depicts that $\text{O}-\text{H}\cdots\text{Se}$ interaction is accompanied by a large increase in density around the oxygen lone pair and density depletion region around the selenium atom as compared to those observed for the corresponding $\text{Se}\cdots\text{O}$ bonded complex.

Comparison between Oxygen and Nitrogen as Electron Donors. Replacing oxygen with nitrogen results in a minor alteration in the geometrical parameters for most of the molecular pairs. As discussed previously, in case of H_2O , true minima was not obtained for few dimers involved in $\text{Se}\cdots\text{O}$ interactions while true minima was obtained for all the structures involved in $\text{Se}\cdots\text{N}$ noncovalent contacts. In terms of the binding energy, nitrogen clearly proved to be a better donor than oxygen as the energy of the $\text{Se}\cdots\text{N}$ interaction was higher than the corresponding $\text{Se}\cdots\text{O}$ interaction for all the interacting pairs. The enhancement in binding energy was observed to be more profound for $\text{XHSe}\cdots\text{O}/\text{N}$ complexes as compared to $\text{XMeSe}\cdots\text{O}/\text{N}$ interaction. The energy decomposition analysis showed that the contribution of the exchange energy was higher in case of the nitrogen donor in comparison to the oxygen donor for most of the cases while their was a decrease in the electrostatic contribution for the nitrogen donors. In case of the molecular pairs involving XMeSe , a bcp was not observed for the existence of an $\text{O}\cdots\text{H}$ interaction in case of $\text{X} = -\text{F}$ (for interaction with OH_2), a bcp for $\text{N}\cdots\text{H}$ interaction was not observed for $\text{X} = -\text{F}, -\text{Cl}, -\text{OH}$, and $-\text{OCH}_3$ (for interaction with NH_3). $E(2)$ energies were also higher for $\text{Se}\cdots\text{N}$ contact than the corresponding values for $\text{Se}\cdots\text{O}$ contact. Figure 16 shows the electron density difference map for $\text{Se}\cdots\text{O}$ and $\text{Se}\cdots\text{N}$ contact for fluorine substituted complexes. In the case of H_2O , their is an increase in the

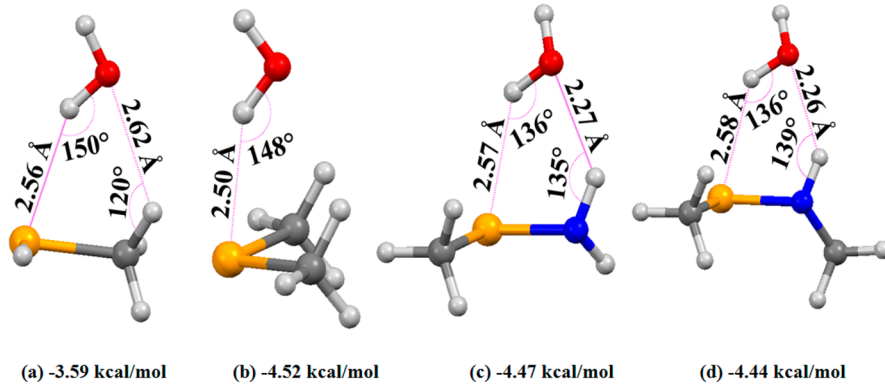


Figure 14. Optimized structure of (a) HMeSe/OH₂, (b) CH₃MeSe/OH₂, (c) NH₂MeSe/OH₂, and (d) CH₃NHMeSe/OH₂ having true minima.

Table 7. Topological Parameters for Optimized Structure of (a) HMeSe/OH₂, (b) CH₃MeSe/OH₂, (c) NH₂MeSe/OH₂, and (d) CH₃NHMeSe/OH₂.

interaction	ρ (e/Å ³)	$\nabla^2\rho$ (e/Å ³)
H···Se	0.098	0.903
	0.042	0.728
CH ₃ MeSe···H ₂ O	0.122	0.973
	0.108	0.896
O···H	0.085	1.057
	0.087	1.074
NH ₂ MeSe···H ₂ O	0.107	0.886
	0.087	1.074
NCH ₃ MeSe···H ₂ O	0.107	0.886
	0.087	1.074

density on the oxygen lone pair and a reduction in density is observed on the hydrogens of H₂O. Also there is a substantial decrease in the density on the right-hand side of the electron accepting Se atom. Besides this, the lone pair on fluorine also experiences an increase in the density with the formation of an Se···O contact [Figure 16, parts a and b]. As compared to this, in case of Se···N contact, the density depleted region on Se and that of NH₃ get combined into one entity and the increase in density on nitrogen lone pair is trapped into this enlarged

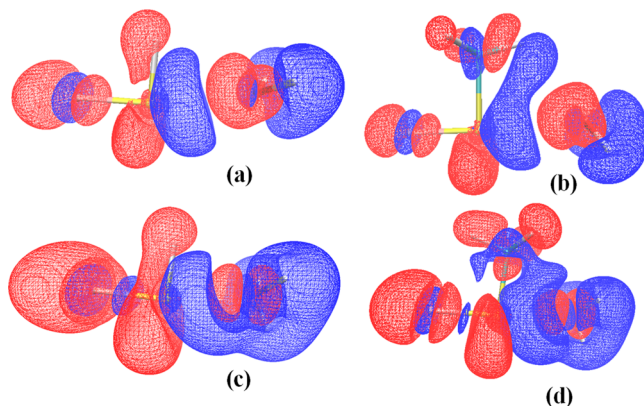


Figure 16. Electron density shift for (a) FHSe···OH₂, (b) FMeSe···OH₂, (c) FHSe···NH₃, and (d) FMeSe···NH₃.

density depleted region. As compared to Se···O, the increase of density on fluorine lone pair is [Figure 16, parts c and d] greater in Se···N contact resulting in stronger Se···N contacts as compared to Se···O contacts.

CONCLUSIONS

A systematic study was performed to study the nature of intermolecular Se···O and Se···N noncovalent bonds. The results indicate that the strength of the Se···O/N contact is

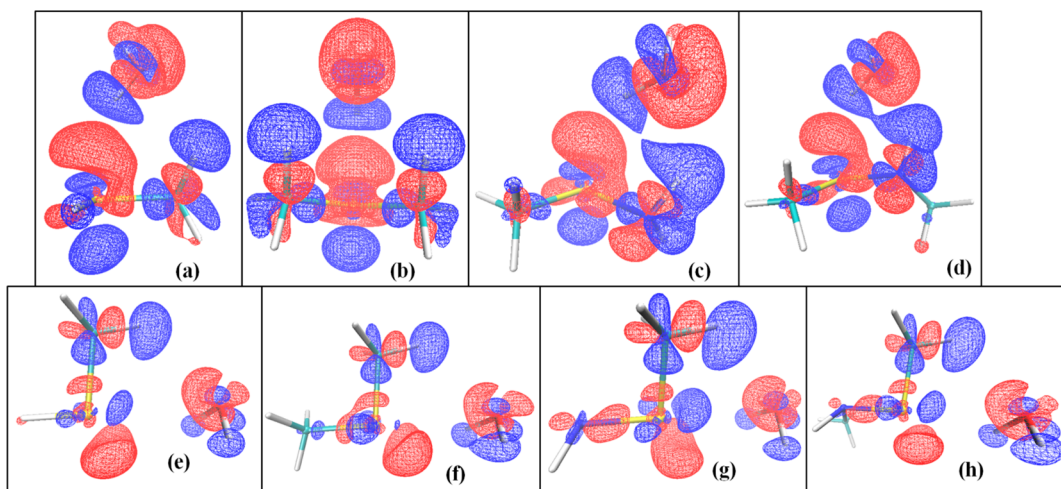


Figure 15. Electron density shift for hydrogen bonding in (a) HMeSe/OH₂, (b) CH₃MeSe/OH₂, (c) NH₂MeSe/OH₂, and (d) NHCH₃MeSe/OH₂ and Se···O contact in (e) H₂Se/OH₂, (f) CH₃HSe/OH₂, (g) NH₂MeSe/OH₂, and (h) NHCH₃MeSe/OH₂.

significantly dependent on the electron withdrawing and electron donating capabilities of substituent X attached to selenium. The replacement of the H atom of XHSe with Me modified the strength of the Se···O/N interaction because of the formation of hydrogen bonding. Furthermore, an increase in the linearity of X···Se···O/N bond in the presence of Me was also observed. A decrease in the binding energy was observed for all Se···O and Se···N contacts when the H atom was replaced by Me. A topological analysis shows that Se···O/N interaction shows similar characteristics as hydrogen bonding. The topological parameters, namely ρ and $\nabla^2\rho$, shows exponential decay with increasing bond path length. Also similar to hydrogen bonds, the IV_bI/G_b ratio exhibits a value closer to 1. It was also observed that mere fulfillment of the geometrical criteria for a noncovalent contact does not necessitate the existence of a bond. Between the atoms, oxygen and nitrogen, nitrogen was clearly established to be a better electron donor and hence formed a strong noncovalent bond with Se as compared to oxygen. Also in some cases involving H_2O as electron donor, hydrogen bonding was more stabilized than the Se···O contact. Electron density difference map clearly depicts that large charge difference occurs in case of hydrogen bonding as compared to the corresponding Se···O contacts. Also in comparing Se···O and Se···N contacts with fluorine substituent the charge enhanced red region of the nitrogen is trapped. These results can be useful in designing selenium containing biomolecules to understand its binding properties and to tune the nature of such binding by changing the chemical environment around selenium. This is expected to have ramifications in the biological function of different classes of molecules containing selenium as a key atomic entity.

■ ASSOCIATED CONTENT

Supporting Information

The Supporting Information is available free of charge on the ACS Publications website at DOI: [10.1021/acs.jpcb.5b08684](https://doi.org/10.1021/acs.jpcb.5b08684).

Coordinates of optimized dimers, molecular electrostatic potential maps, plots of bond critical point between dimers, results of energy decomposition analysis of Se···O/N bond, and properties of O–H···Se and C–H···O hydrogen bonds ([DOCX](#))

■ AUTHOR INFORMATION

Corresponding Author

*(D.C.) E-mail: dchopra@iiserb.ac.in. Fax: 91-755-6692392.

Notes

The authors declare no competing financial interest.

■ ACKNOWLEDGMENTS

R.S. thanks the DST for an INSPIRE-PhD fellowship. R.S. also thanks Kunal Kishore for his help in computational calculations. D.C. thanks IISER Bhopal for providing infrastructural and computational facilities.

■ REFERENCES

- Xu, J. F.; Chen, L.; Zhang, X. How to Make Weak Noncovalent Interactions Stronger. *Chem. - Eur. J.* **2015**, *21*, 11938.
- Zheng, Y. Z.; Deng, G.; Zhou, Y.; Sun, H. Y.; Yu, Z. W. Comparative Study of Halogen- and Hydrogen-Bond Interactions between Benzene Derivatives and Dimethyl Sulfoxide. *ChemPhysChem* **2015**, *16*, 2594–2601.

(3) Dai, Y.; Guo, M.; Peng, J.; Shen, W.; Li, M.; He, R.; Zhu, C.; Lin, S. H. Noncovalent Interaction and its Influence on Excited-State Behavior: A Theoretical Study on the Mixed Coaggregates of Dicyanophthalene and Pyrazoline. *Chem. Phys. Lett.* **2013**, *556*, 230–236.

(4) Saha, S.; Sastry, G. N. Cooperative or Anticooperative: How Noncovalent Interactions Influence Each Other. *J. Phys. Chem. B* **2015**, *119*, 11121.

(5) Johnson, E. R.; Keinan, S.; Mori-Sánchez, P.; Contreras-García, J.; Cohen, A. J.; Yang, W. Revealing Noncovalent Interactions. *J. Am. Chem. Soc.* **2010**, *132*, 6498–6506.

(6) Riley, K. E.; Hobza, P. Noncovalent Interactions in Biochemistry. *WIREs Comput. Mol. Sci.* **2011**, *1*, 3–17.

(7) Zhu, H.; Sommer, I.; Lengauer, T.; Domingues, F. S. Alignment of Non-Covalent Interactions at Protein-Protein Interfaces. *PLoS One* **2008**, *3*, e1926.

(8) Gurusaran, M.; Shankar, M.; Nagarajan, R.; Helliwell, J. R.; Sekar, K. Do We See What We Should See? Describing non-covalent Interactions in Protein Structures Including Precision. *IUCrJ* **2014**, *1*, 74–81.

(9) Ball, V.; Maechling, C. Isothermal Microcalorimetry to Investigate Non Specific Interactions in Biophysical Chemistry. *Int. J. Mol. Sci.* **2009**, *10*, 3283–3315.

(10) Zondlo, N. J. Fold Globally, Bond Locally. *Nat. Chem. Biol.* **2010**, *6*, 567–568.

(11) Desiraju, G. R. Hydrogen Bridges in Crystal Engineering: Interactions without Borders. *Acc. Chem. Res.* **2002**, *35*, 565–573.

(12) Desiraju, G. R.; Steiner, T. *The Weak Hydrogen Bond in Structural Chemistry and Biology*; Oxford University Press: Oxford, U.K., 1999.

(13) Prins, L. P.; Reinoudt, D. N.; Timmerman, P. Noncovalent Synthesis Using Hydrogen Bonding. *Angew. Chem., Int. Ed.* **2001**, *40*, 2382–2426.

(14) Hubbard, R. E.; Kamran Haider, M. Hydrogen Bonds in Proteins: Role and Strength. In *eLS*; John Wiley & Sons, Ltd.: New York, 2001.

(15) Bowie, J. U. Membrane Protein Folding: How Important are Hydrogen Bonds? *Curr. Opin. Struct. Biol.* **2011**, *21*, 42–49.

(16) Rajagopal, S.; Vishveshwara, S. Short Hydrogen Bonds in Proteins. *FEBS J.* **2005**, *272*, 1819–1832.

(17) Ben-Naim, A. The Role of Hydrogen Bonds in Protein Folding and Protein Association. *J. Phys. Chem.* **1991**, *95*, 1437–1444.

(18) McGaughey, G. B.; Gagné, R.; Rappé, A. K. π -Stacking Interactions Alive and Well in Proteins. *J. Biol. Chem.* **1998**, *273*, 15458–15463.

(19) Churchill, C. D. M.; Navarro-Whyte, L.; Rutledge, L. R.; Wetmore, S. D. Effects of the Biological Backbone on DNA–protein Stacking Interactions. *Phys. Chem. Chem. Phys.* **2009**, *11*, 10657–10670.

(20) Swart, M.; van der Wijst, T.; Fonseca Gueraa, C.; Bickelhaupt, F. M. π - π Stacking Tackled with Density Functional Theory. *J. Mol. Model.* **2007**, *13*, 1245–1257.

(21) Martinez, C. R.; Iverson, B. L. Rethinking the term “Pi-Stacking”. *Chem. Sci.* **2012**, *3*, 2191.

(22) Grimme, S. Do Special Noncovalent π - π Stacking Interactions Really Exist? *Angew. Chem., Int. Ed.* **2008**, *47*, 3430–3434.

(23) Auffinger, P.; Hays, F. A.; Westhof, E.; Ho, P. S. Halogen Bonds in Biological Molecules. *Proc. Natl. Acad. Sci. U. S. A.* **2004**, *101*, 16789–16794.

(24) Voth, A. R.; Khuu, P.; Oishi, K.; Ho, P. S. Halogen Bonds as Orthogonal Molecular Interactions to Hydrogen Bonds. *Nat. Chem.* **2009**, *1*, 74–79.

(25) Wilcken, R.; Zimmermann, M. O.; Lange, A.; Joerger, A. C.; Boeckler, F. M. Principles and Applications of Halogen Bonding in Medicinal Chemistry and Chemical Biology. *J. Med. Chem.* **2013**, *56*, 1363–1388.

(26) Politzer, P.; Murray, J. S.; Clark, T. Halogen Bonding and Other σ -hole Interactions: A Perspective. *Phys. Chem. Chem. Phys.* **2013**, *15*, 11178.

- (27) Metrangolo, P.; Meyer, F.; Pilati, T.; Resnati, G.; Terraneo, G. Halogen Bonding in Supramolecular Chemistry. *Angew. Chem., Int. Ed.* **2008**, *47*, 6114–6127.
- (28) Mani, D.; Arunan, E. The X–C···Y (X = O/F, Y = O/S/F/Cl/Br/N/P) ‘Carbon Bond’ and Hydrophobic Interactions. *Phys. Chem. Chem. Phys.* **2013**, *15*, 14377–14383.
- (29) Escudero-Adán, E. C.; Bauzá, A.; Frontera, A.; Ballester, P. Nature of Noncovalent Carbon-Bonding Interactions Derived from Experimental Charge-Density Analysis. *ChemPhysChem* **2015**, *16*, 2530.
- (30) Thomas, S. P.; Pavan, M. S.; Guru Row, T. N. Experimental Evidence for ‘Carbon Bonding’ in the Solid State from Charge Density Analysis. *Chem. Commun.* **2014**, *50*, 49–51.
- (31) Wang, W.; Ji, B.; Zhang, Yu. Chalcogen Bond: A Sister Noncovalent Bond to Halogen Bond. *J. Phys. Chem. A* **2009**, *113*, 8132–8135.
- (32) Garrett, G. E.; Gibson, G. L.; Straus, R. N.; Seferos, D. S.; Taylor, M. S. Chalcogen Bonding in Solution: Interactions of Benzotelluradiazoles with Anionic and Uncharged Lewis Bases. *J. Am. Chem. Soc.* **2015**, *137*, 4126–4133.
- (33) Tsuzuki, S.; Sato, N. Origin of Attraction in Chalcogen–Nitrogen Interaction of 1,2,5-Chalcogenadiazole Dimers. *J. Phys. Chem. B* **2013**, *117*, 6849–6855.
- (34) Zahn, S.; Frank, R.; Hey-Hawkins, E.; Kirchner, B. Pnicogen Bonds: A New Molecular Linker. *Chem. - Eur. J.* **2011**, *17*, 6034–6038.
- (35) Sarkar, S.; Pavan, M. S.; Guru Row, T. N. G. Experimental Validation of ‘Pnicogen Bonding’ in Nitrogen by Charge Density Analysis. *Phys. Chem. Chem. Phys.* **2015**, *17*, 2330–2334.
- (36) Guan, L.; Mo, Y. Electron Transfer in Pnicogen Bonds. *J. Phys. Chem. A* **2014**, *118*, 8911–8921.
- (37) Esrafil, M. D.; Mohammadian-Sabet, F. Cooperative Effects in Hydrogen Bond and Pnicogen Bond: A Comparative Study. *Can. J. Chem.* **2014**, *92*, 1151–1156.
- (38) Adhikari, U.; Scheiner, S. Sensitivity of Pnicogen, Chalcogen, Halogen and H-bonds to Angular Distortions. *Chem. Phys. Lett.* **2012**, *532*, 31–35.
- (39) Scheiner, S. The Pnicogen Bond: Its Relation to Hydrogen, Halogen, and Other Noncovalent Bonds. *Acc. Chem. Res.* **2013**, *46*, 280–288.
- (40) Scheiner, S. Sensitivity of Noncovalent Bonds to Intermolecular Separation: Hydrogen, Halogen, Chalcogen, and Pnicogen Bonds. *CrystEngComm* **2013**, *15*, 3119–3124.
- (41) Jacob, C.; Giles, G. I.; Giles, N. M.; Sies, H. Sulfur and Selenium: The Role of Oxidation State in Protein Structure and Function. *Angew. Chem., Int. Ed.* **2003**, *42*, 4742–4758.
- (42) Metrangolo, P.; Resnati, G. Halogen and Chalcogen Team Up. *Nat. Chem.* **2012**, *4*, 437–438.
- (43) Engman, L.; Stern, D.; Frisell, H.; Vessman, K.; Berglund, M.; Ek, B.; Andersson, C. G. Synthesis, Antioxidant Properties, Biological Activity and Molecular Modelling of a Series of Chalcogen Analogues of the 5-Lipoxygenase Inhibitor DuP 654. *Bioorg. Med. Chem.* **1995**, *3*, 1255–1262.
- (44) Manjare, S. T.; Kim, Y.; Churchill, D. G. Selenium- and Tellurium-Containing Fluorescent Molecular Probes for the Detection of Biologically Important Analytes. *Acc. Chem. Res.* **2014**, *47*, 2985–2998.
- (45) Clark, T.; Murray, J. S.; Lane, P.; Politzer, P. Why are Dmethyl Sulfoxide and Dimethyl Sulfone Such Good Solvents? *J. Mol. Model.* **2008**, *14*, 689–697.
- (46) Politzer, P.; Murray, J. S.; Concha, M. C. σ -hole Bonding Between like Atoms; a Fallacy of Atomic Charges. *J. Mol. Model.* **2008**, *14*, 659–665.
- (47) Murray, J. S.; Lane, P.; Politzer, P. Simultaneous σ -Hole and Hydrogen Bonding by Sulfur- and Selenium- Containing Heterocycles. *Int. J. Quantum Chem.* **2008**, *108*, 2770–2781.
- (48) Das, D.; Singh, P.; Singh, M.; Singh, A. K. Tetridentate Selenium Ligand as a Building Block for Homodinuclear Complexes of Pd(II) and Ru(II) Having Seven Membered Rings or Bis-Pincer Coordination Mode: High Catalytic Activity of Pd-Complexes for Heck Reaction. *Dalton Trans.* **2010**, *39*, 10876–10882.
- (49) Nishibayashi, Y.; Uemura, S. Selenium Compounds as Ligands and Catalysts. *Top. Curr. Chem.* **2000**, *208*, 235–255.
- (50) Kumar, A.; Rao, G. K.; Saleem, F.; Singh, A. K. Organoselenium Ligands in Catalysis. *Dalton Trans.* **2012**, *41*, 11949–11977.
- (51) Martin, C. D.; Ragogna, P. J. Oxygen, Sulfur, Selenium, Tellurium and Polonium. *Annu. Rep. Prog. Chem., Sect. A: Inorg. Chem.* **2011**, *107*, 110–124.
- (52) Tiecco, M.; Testaferrri, L.; Santi, C.; Tomassini, C.; Santoro, S.; Marini, F.; Bagnoli, L.; Temperini, A.; Costantino, F. Intramolecular Nonbonding Interactions between Selenium and Sulfur – Spectroscopic Evidence and Importance in Asymmetric Synthesis. *Eur. J. Org. Chem.* **2006**, *2006*, 4867–4873.
- (53) Morella, A. M.; Ward, A. D. The *Cis* Chlorination of Alkenes Using Selenium Reagents. *Tetrahedron Lett.* **1984**, *25*, 1197–1200.
- (54) Wirth, T. Chiral Selenium Compounds: Versatile Reagents in Organic Synthesis. *Liebigs Ann./Recueil* **1997**, *1997* (11), 2189–2196.
- (55) Balkrishna, S. J.; Kumar, S.; Azad, G. K.; Bhakuni, B. S.; Panini, P.; Ahalawat, N.; Tomar, R. S.; Detty, M. R.; Kumar, S. An Ebselen like Catalyst with Enhanced GPx Activity via a Selenol Intermediate. *Org. Biomol. Chem.* **2014**, *12*, 1215–1219.
- (56) Balkrishna, S. J.; Bhakuni, B. S.; Kumar, S. Copper Catalyzed/Mediated Synthetic Methodology for Ebselen and Related Isoselenazolones. *Tetrahedron* **2011**, *67*, 9565–9575.
- (57) Mugesh, G.; du Mont, W. W.; Sies, H. Chemistry of Biologically Important Synthetic Organoselenium Compounds. *Chem. Rev.* **2001**, *101*, 2125–2180.
- (58) Mugesh, G.; Singh, H. B. Synthetic Organoselenium Compounds as Antioxidants: Glutathioneperoxidase Activity. *Chem. Soc. Rev.* **2000**, *29*, 347–357.
- (59) Santoro, S.; Azeredo, J. B.; Nascimento, V.; Sancinetto, L.; Braga, A. L.; Santi, C. The Green Side of the Moon: Ecofriendly Aspects of Organoselenium Chemistry. *RSC Adv.* **2014**, *4*, 31521–31535.
- (60) Yu, L.; Li, H.; Zhang, Xu.; Ye, J.; Liu, J.; Xu, Q.; Lautens, M. Organoselenium-Catalyzed Mild Dehydration of Aldoximes: An Unexpected Practical Method for Organonitrile Synthesis. *Org. Lett.* **2014**, *16*, 1346–1349.
- (61) Chow, O.; Barbul, A. Immunonutrition: Role in Wound Healing and Tissue Regeneration. *Adv. Wound Care* **2014**, *3*, 46–53.
- (62) Carlson, B. A.; Yoo, M. K.; Shrimali, R. K.; Irons, R.; Gladyshev, V. N.; Hatfield, D. L.; Park, J. M. Micronutrients and the Immune System. Role of Selenium-Containing Proteins in T-cell and Macrophage Function. *Proc. Nutr. Soc.* **2010**, *69*, 300–310.
- (63) Frost, D. V.; Lish, P. M. Selenium in Biology. *Annu. Rev. Pharmacol.* **1975**, *15*, 259–284.
- (64) Zhao, J.; Pu, Y.; Gao, Y.; Peng, X.; Li, Y.; Xu, X.; Li, B.; Zhu, N.; Dong, J.; Wu, G.; Li, Y.F. Identification and Quantification of Selenoproteins by 2-DE-SR-XRF in Selenium-Enriched Yeasts. *J. Anal. At. Spectrom.* **2015**, *30*, 1408.
- (65) Kieliszek, M.; Błażejek, S.; Bzducha-Wróbel, A. Influence of Selenium Content in the Culture Medium on Protein Profile of Yeast Cells *Candida utilis* ATCC. *Oxid. Med. Cell. Longevity* **2015**, *2015*, 1–6.
- (66) Behne, D.; Kyriakopoulos, A. Mammalian Selenium-Containing Proteins. *Annu. Rev. Nutr.* **2001**, *21*, 453–73.
- (67) Chen, Y. C.; Prabhu, K. S.; Mastro, A. M. Is Selenium a Potential Treatment for Cancer Metastasis? *Nutrients* **2013**, *5*, 1149–1168.
- (68) Misra, S.; Boylan, M.; Selvam, A.; Spallholz, J. E.; Björnstedt, M. Redox-Active Selenium Compounds—From Toxicity and Cell Death to Cancer Treatment. *Nutrients* **2015**, *7*, 3536–3556.
- (69) Srivastava, K.; Chakraborty, T.; Singh, H. K.; Butcher, R. J. Intramolecularly Coordinated Azobenzene Selenium Derivatives: Effect of Strength of the Se···N Intramolecular Interaction on luminescence. *Dalton Trans.* **2011**, *40*, 4489.
- (70) Mugesh, G.; Panda, A.; Singh, H. B.; Butcher, R. J. Intramolecular Se···N Nonbonding Interaction in Low-Valent Organoselenium Derivatives: A Detailed Study by ^1H , ^{77}Se NMR Spectroscopy and X-ray Crystallography. *Chem. - Eur. J.* **1999**, *5*, 1411–1421.

- (71) Singh, B. G.; Thomas, E.; Sawant, S. N.; Takahashi, K.; Dedachi, K.; Iwaoka, M.; Priyadarsini, K. I. Radical Cations of Aromatic Selenium Compounds: Role of Se···X Nonbonding Interactions. *J. Phys. Chem. A* **2013**, *117*, 9259–9265.
- (72) Mukherjee, A. J.; Zade, S. S.; Singh, H. B.; Sunoj, R. B. Organoselenium Chemistry: Role of Intramolecular Interactions. *Chem. Rev.* **2010**, *110*, 4357–4416.
- (73) Kandasamy, K.; Kumar, S.; Singh, H. B.; Butcher, R. J.; Holman, K. T. Synthesis, Structural Characterization and Fluorescence Properties of Organoselenium Compounds Bearing a Ligand Containing Both Steric and Nonbonded Interacting Groups. First Unusual Observation of Both Se···N and Se···O Intramolecular Interactions in a Diselenide Structure. *Eur. J. Inorg. Chem.* **2004**, *2004*, 1014–1023.
- (74) Linden, A.; Zhou, Y.; Heimgartner, H. Intra- and Intermolecular Se···X (X = Se, O) Interactions in Selenium-containing Heterocycles: Benzoylimino-5-(morpholin-4-yl)-1,2,4-diselenazole. *Acta Crystallogr., Sect. C: Struct. Chem.* **2014**, *70*, 482–487.
- (75) Brezgunova, M. E.; Lieffrig, J.; Aubert, E.; Dahaoui, S.; Fertey, P.; Lebègue, S.; Ángyan, J. G.; Fourmigé, M.; Espinosa, E. Chalcogen Bonding: Experimental and Theoretical Determinations from Electron Density Analysis. Geometrical Preferences Driven by Electrophilic–Nucleophilic Interactions. *Cryst. Growth Des.* **2013**, *13*, 3283–3289.
- (76) Thomas, S. P.; Satheeshkumar, K.; Mugesh, G.; Guru Row, T. N. Unusually Short Chalcogen Bonds Involving Organoselenium: Insights into the Se–N Bond Cleavage Mechanism of the Antioxidant Ebselein and Analogue. *Chem. - Eur. J.* **2015**, *21*, 6793–6800.
- (77) Pati, P. B.; Zade, S. S. Benzoselenadiazole Containing Donor–Acceptor–Donor Small Molecules: Nonbonding Interactions, Packing Patterns, and Optoelectronic Properties. *Cryst. Growth Des.* **2014**, *14*, 1695–1700.
- (78) Balkrishna, S. J.; Shukla, R.; Jasinski, J. P.; Kumar, S. Crystal Structure Studies on Some of Benzamide Ring Substituted Isoselenazolones and Symmetric Diaryl Monoselenides Derived from Benzamides. *Proc. Natl. Acad. Sci., India, Sect. A* **2014**, *84*, 165–177.
- (79) Berionni, G.; Pégot, B.; Marrot, J.; Goumont, R. Supramolecular association of 1,2,5-chalcogenadiazoles: An Unexpected Self-Assembled Dissymmetric [Se···N]₂ Four-Membered Ring. *CrystEngComm* **2009**, *11*, 986–988.
- (80) Head-Gordon, M.; Pople, J. A.; Frisch, M. J. MP2 energy evaluation by direct methods. *Chem. Phys. Lett.* **1988**, *153*, 503–506.
- (81) Kendall, R. A.; Dunning, T. H., Jr.; Harrison, R. J. Electron Affinities of the First-Row Atoms Revisited. Systematic Basis Sets and Wave Functions. *J. Chem. Phys.* **1992**, *96*, 6796–6806.
- (82) Hauchecorne, D.; Herrebout, W. A. Experimental Characterization of C–X···Y–C (X = Br, I; Y = F, Cl) Halogen–Halogen Bonds. *J. Phys. Chem. A* **2013**, *117*, 11548–11557.
- (83) Scheiner, S. Effects of Substituents upon the P···N Noncovalent Interaction: The Limits of Its Strength. *J. Phys. Chem. A* **2011**, *115*, 11202–11209.
- (84) Wu, J. Structure, Properties, and Nature of the BrF–HX Complexes: An Ab Initio Study. *Int. J. Quantum Chem.* **2011**, *111*, 4247–4254.
- (85) Adhikari, U.; Scheiner, S. Effects of Charge and Substituent on the S···N Chalcogen Bond. *J. Phys. Chem. A* **2014**, *118*, 3183–3192.
- (86) Frisch, M. J.; Trucks, G. W.; Schlegel, H. B.; Scuseria, G. E.; Robb, M. A.; Cheeseman, J. R.; Scalmani, G.; Barone, V.; Mennucci, B.; Petersson, G. A.; et al. *Gaussian 09*, Revision D.01, Gaussian, Inc.: Wallingford, CT, 2009.
- (87) Boys, S. F.; Bernardi, F. The Calculation of Small Molecular Interactions by the Differences of Separate Total Energies. Some Procedures with Reduced Errors. *Mol. Phys.* **1970**, *19*, 553–566.
- (88) Keith, T. A. AIMALL, version 13.05.06, TK Gristmill Software: Overland Park, KS, 2013; aim.tkgristmill.com.
- (89) Reed, A. E.; Curtiss, L. A.; Weinhold, F. Intermolecular Interactions from a Natural Bond Orbital, Donor-Acceptor Viewpoint. *Chem. Rev.* **1988**, *88*, 899–926.
- (90) Reed, A. E.; Weinhold, F.; Curtiss, L. A.; Pochatko, D. J. Natural Bond Orbital Analysis of Molecular Interactions: Theoretical Studies of Binary Complexes of HF, H₂O, NH₃, N₂, O₂, F₂, CO and CO₂ with HF, H₂O, and NH₃. *J. Chem. Phys.* **1986**, *84*, 5687–5705.
- (91) Glendening, E. D.; Badenhoop, J. K.; Reed, A. E.; Carpenter, J. E.; Bohmann, J. A.; Morales, C. M.; Landis, C. R.; Weinhold, F. *NBO 6.0*; Theoretical Chemistry Institute, University of Wisconsin: Madison, WI, 2013.
- (92) Schmidt, M. W.; Baldridge, K. K.; Boatz, J. A.; Elbert, S. T.; Gordon, M. S.; Jensen, J. H.; Koseki, S.; Matsunaga, N.; Nguyen, K. A.; Su, S.; et al. General Atomic and Molecular Electronic Structure System. *J. Comput. Chem.* **1993**, *14*, 1347–1363.
- (93) Gordon, M. S.; Schmidt, M. W. Advances in Electronic Structure Theory: GAMESS a Decade Later. In *Theory and Applications of Computational Chemistry: The First Forty Years*; Dykstra, C. E., Frenking, G., Kim, K. S., Scuseria, G. E., Eds.; Elsevier: Amsterdam, 2005; pp 1167–1189.
- (94) Su, P.; Jiang, Z.; Chen, Z.; Wu, W. Energy Decomposition Scheme Based on the Generalized Kohn–Sham Scheme. *J. Phys. Chem. A* **2014**, *118*, 2531–2542.
- (95) Yu, F. Intermolecular Interactions of Formic Acid with Benzene: Energy Decomposition Analyses with Ab Initio MP2 and Double-Hybrid Density Functional Computations. *Int. J. Quantum Chem.* **2013**, *113*, 2355–2360.
- (96) Chen, Y.; Li, H. Intermolecular Interaction in Water Hexamer. *J. Phys. Chem. A* **2010**, *114*, 11719–11724.
- (97) Feller, D. The Role of Databases in Support of Computational Chemistry Calculations. *J. Comput. Chem.* **1996**, *17*, 1571–1586.
- (98) Schuchardt, K. L.; Didier, B. T.; Elsethagen, T.; Sun, L.; Gurumoorthy, V.; Chase, J.; Li, J.; Windus, T. L. Basis Set Exchange: A Community Database for Computational Sciences. *J. Chem. Inf. Model.* **2007**, *47*, 1045–1052.
- (99) Lu, T.; Chen, F. Multiwfn: A multifunctional wavefunction analyzer. *J. Comput. Chem.* **2012**, *33*, 580–592.
- (100) Humphrey, W.; Dalke, A.; Schulten, K. VMD – Visual Molecular Dynamics. *J. Mol. Graphics* **1996**, *14*, 33–38.
- (101) Alikhani, E.; Fuster, F.; Madebene, B.; Grabowski, S. Topological Reaction Sites – Very Strong Chalcogen Bonds. *Phys. Chem. Chem. Phys.* **2014**, *16*, 2430–2442.
- (102) Popelier, P. L. A. *J. Phys. Chem. A* **1998**, *102*, 1873–1878.
- (103) Arunan, E.; Desiraju, G. R.; Klein, R. A.; Sadlej, J.; Scheiner, S.; Alkorta, I.; Clary, D. C.; Crabtree, R. H.; Dannenberg, J. J.; Hobza, P.; et al. Definition of the Hydrogen Bond. *Pure Appl. Chem.* **2011**, *83*, 1637–1641.